First-principles study of the iron pnictide superconductor BaFe$_2$As$_2$

E. Aktürk[1] and S. Ciraci[1,2,*]

[1]*UNAM-Institute of Materials Science and Nanotechnology, Bilkent University, Ankara 06800, Turkey*
[2]*Department of Physics, Bilkent University, Ankara 06800, Turkey*

This paper presents our study on the atomic, electronic, magnetic structures, and phonon modes of the low-temperature orthorhombic phase of undoped BaFe$_2$As$_2$ crystal. The electronic structure is characterized by a sharp Fe-3d peak close to the Fermi level and is dominated by Fe-3d- and As-4p-hybridized states. Ba contribution occurs only at lower energies. The spin ordering of the magnetic ground state, which is determined by minimizing the total energy of different spin alignments on Fe atoms in the conventional cell, is in agreement with experimental findings but is different from the antiferromagnetic spin ordering obtained by assigning antiparallel spin directions on two Fe atoms in the primitive unit cell. Valuable information about the charge transfer and bonding is revealed through the analysis of the charge density. Electrons are transferred from Ba to Fe-As layers and also from Fe to As atoms. The magnetic phonon calculations of the ground state are carried out to predict Raman and infrared-active modes. Softening of some calculated spin-dependent phonon modes corroborates the contribution of spin-lattice coupling to the structural phase transition from $I4/mmm$ to $Fmmm$.

I. INTRODUCTION

The superconductor phase occurring at the transition temperature T_c as high as 55 K has initiated active research on iron-oxypnictide compounds.[1] BaFe$_2$As$_2$ has been found to be superconductor up to 38 K upon hole doping by the substitution of potassium for barium.[2] On the other hand, recent experiments predict that BaFe$_2$As$_2$ without doping has been made superconducting under high pressure by about 2–6 GPa.[3] In an effort to understand the mechanism of this superconducting state the atomic structure of parent (undoped) BaFe$_2$As$_2$ compound has been investigated experimentally by Rotter *et al.*[4] It has been found that undoped BaFe$_2$As$_2$ undergoes a structural phase transition at $\sim$140 K from tetragonal $I4/mmm$ symmetry to orthorhombic $Fmmm$ symmetry. The structural phase transition, which is confirmed also by a sharp peak observed in the variation in specific heat,[5] has been shown to strongly affect the electronic and magnetic properties of the crystal.[6] For example, the anomaly in resistivity is related to the structural phase transition.

The magnetic susceptibility of BaFe$_2$As$_2$ exhibits an antiferromagnetic (AFM) spin ordering at $\sim$140 K. The antiferromagnetic ordering has been investigated by neutron powder diffraction[4,7,8] and neutron-scattering[9] experiments on BaFe$_2$As$_2$. Huang *et al.*[7] have also observed a three-dimensional long-range AFM ordering occurring below T $\sim$100 K. It appears that the antiferromagnetism is destroyed upon doping and the metallic state changes into superconducting state. The metallic properties of undoped BaFe$_2$As$_2$ have been revealed at the high plasma frequencies, ω_p $\geq$1.5 eV.[10] Based on density-functional calculation, Yildirim[11] predicted that there is a strong interplay between structural and magnetic properties of Fe-pnictide system where the c axis collapses with the loss of Fe magnetism. In contrast to cuprate superconductors (where localized electrons due to the large Coulomb repulsion give rise to the antiferromagnetic state) the metallicity of BaFe$_2$As$_2$ suggests relatively weaker U and hence spin-density wave rather than localized AFM order.

In this paper we investigate atomic, electronic, magnetic structures, and phonon modes of the low-temperature $Fmmm$ phase of parent-undoped BaFe$_2$As$_2$. For the sake of comparison, we carried out calculations on the tetragonal high-temperature $I4/mmm$ phase. We presented an analysis of charge transfer and bonding between atoms. The ground-state spin ordering determined among six different spin configurations on Fe atoms is antiferromagnetic, but it is ferromagnetic (FM) only along Fe rows in the direction parallel to the shortest vector of orthorhombic lattice. We presented an extensive analysis of electronic structure and charge density. This AFM ground state is metallic with total and orbital projected density of states (DOS) is dominated by Fe-3d- and As-4p-hybridized states near but below the Fermi level. We found that phonon modes calculated for the AFM ground state at the center of the Brillouin zone (BZ) are compared with those observed experimentally. We believe that our findings are crucial for the understanding of this class of materials.

II. METHOD

Our results are based on the first-principle plane-wave calculations within generalized gradient approximation using Perdew-Burke-Enzerhof. The band theory is applicable for iron pnictides, since the effective U (which is estimated to be less than 0.5) is reduced by hybridization of localized Fe-3d electrons with As-4p electrons. We use ultrasoft pseudopotentials[12] and plane-wave basis set with kinetic-energy cutoff $\hbar^2|\mathbf{k}+\mathbf{G}|^2/2m$=476 eV. Numerical results have been obtained by using plane-wave self-consistent field (PWSCF) code.[13] In the self-consistent potential, total energy, and other calculations, the BZ is sampled in the **k** space within Monkhorst-Pack scheme.[14] The numbers of these k points
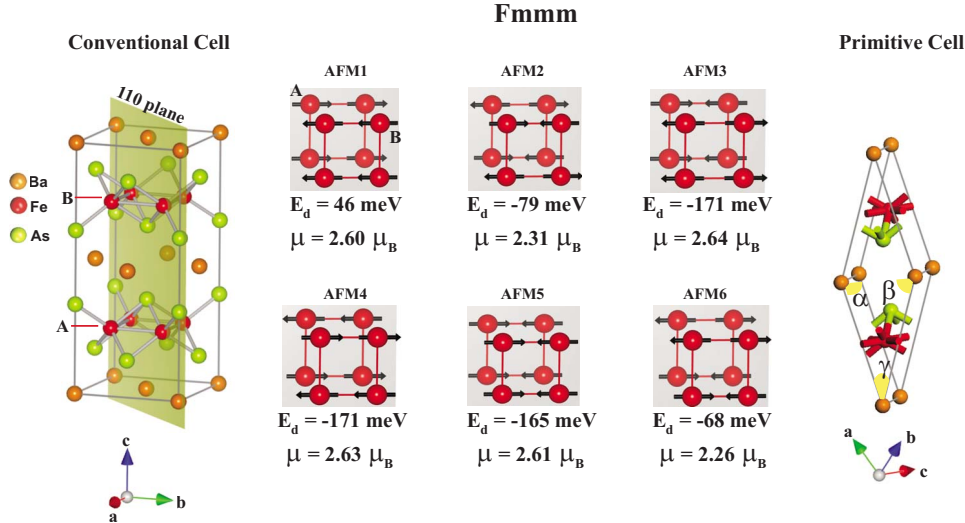
Fmmm

FIG. 1. (Color online) Optimized atomic structure of the low-temperature phase of $BaFe_2As_2$ having orthorhombic *Fmmm* symmetry. AFM1,...,AFM6 are six different spin configurations in the conventional unit cell. Primitive unit cells of crystal structure is also shown. The antiferromagnetic state specified as AFM2 can also be obtained by assigning opposite spins to two Fe atoms in the primitive cell at the right hand side of the figure. This AFM2 state is an excited state with an energy 92 meV/Fe higher relative to the true AFM ground state corresponding the spin configurations either AFM3 or AFM4. The energy of nonmagnetic state is taken to be zero. Lattice vectors a, b, and c of the conventional and primitive cells are shown. Units of the total energy relative to the nonmagnetic state, E_d and the magnetic moment, μ are meV/Fe and μ_B/Fe, respectively.

are $(6 \times 6 \times 3)$ for *Fmmm*, and $(9 \times 9 \times 3)$ for *I4/mmm*, respectively. Atomic positions in all structures are optimized.[15] Convergence of structure optimizations is achieved when the difference of the total energies of last two consecutive steps is less than 10^{-6} eV, the maximum force allowed on each atom is less than 10^{-3} eV/Å, and the pressure is less than 0.05 kbar. In addition to full structure optimization, calculations of phonon modes within linear-response theory[13] yielded positive phonon frequencies for all modes, and hence confirmed the stability of the low-temperature $BaFe_2As_2$ structure.

III. RESULTS

A. Optimized lattice parameters

The structure of $BaFe_2As_2$ in orthorhombic *Fmmm* symmetry is optimized for the FM, AFM, and nonmagnetic (NM) states. The AFM spin ordering is determined among six possible complex spin configurations on Fe atoms in different layers as shown in Fig. 1. We found that the spin configurations AFM3 and AFM4 correspond to the ground state for *Fmmm* orthorhombic phase. The other excited configurations, AFM1, AFM2, AFM5, and AFM6 have energies of 217, 92, 6, and 103 meV/Fe higher than the ground state. The ground-state spin ordering specified as AFM3 is complex and is antiferromagnetic between adjacent Fe layers, which are parallel to the (001) plane. However, in each Fe plane the spin ordering continues to be antiferromagnetic in Fe rows parallel to the lattice vector **a**, while it becomes ferromagnetic in Fe rows along the shortest lattice vector **b**. The magnitude of magnetic moment on each Fe atoms is calculated to be $\sim 2.6\mu_B$ for ground-state spin configuration, but the total magnetic moment is found to be zero. The pre-

dicted AFM state and its spin order of $BaFe_2As_2$ in *Fmmm* are in agreement with the experimental observations.[7,8] Another magnetic state specified as AFM2 has energy 92 meV/Fe higher than that of AFM3 and has perfect antiferromagnetic spin ordering not only inside the Fe planes but also between adjacent ones. As seen in Fig. 1, the magnetic moments of AFM2, AFM5, and AFM6 spin orderings are, respectively, 2.31, 2.61, and 2.26μ_B/Fe, which are smaller than that of AFM3. It is important to note that earlier calculations have represented the antiferromagnetic state of the *Fmmm* phase in the primitive unit cell (see Fig. 1) by assigning opposite spins to two Fe atoms. However, this magnetic state, which is equivalent to AFM2 state is only an excited state and is 92 meV higher in energy relative to the true excited state AFM3 calculated in the conventional cell.

The total energies and optimized structural parameters of the undoped $BaFe_2As_2$ in *Fmmm* symmetry are presented in Table I for different magnetic states. For the sake of completeness, the calculated data of the nonmagnetic high-temperature phase having *I4/mmm* symmetry are also presented. These structure parameters are in agreement with neutron and x-ray data.[4,7] The As-Fe-As tetrahedral angle and Fe-As distance are smallest for the NM but largest for the FM state, whereas the nearest As-As distance is largest in the AFM state. It is also seen that the calculated c of the nonmagnetic state is 0.54 Å smaller than c measured experimentally for *I4/mmm*.

B. Electronic structure

Earlier the electronic band structure of the high-temperature *I4/mmm* phase of $BaFe_2As_2$ with experimental lattice constants has been thoroughly investigated.[16–21] How-

TABLE I. Optimized structure parameters of the undoped $BaFe_2As_2$ crystal and their total energies calculated for different phases and different magnetic states. The total energies E_d are given relative to the total energy of the NM state calculated for optimized crystal structure. Calculated results for the high-temperature $I4/mmm$ phase in NM state are also given.

				Fmmm				
State	a (Å)	b (Å)	c (Å)	Fe-Fe (Å)	Fe-As (Å)	As-As (Å)	Ba-As (Å)	E_d (meV/Fe)
AFM3	5.696	5.586	12.856	2.84;2.79	2.41	3.92; 3.74	3.359; 3.403	−171
AFM4	5.585	5.691	12.868	2.84;2.79	2.41	3.93; 3.73	3.357; 3.401	−171
AFM2	5.650	5.630	12.780	2.82;2.81	2.39	3.85; 3.79	3.390; 3.394	−79
NM	5.577	5.577	12.470	2.79	2.32	3.70; 3.79	3.370; 3.372	0
Expt.	5.614	5.574	12.950	2.81;2.79	2.39	3.91; 3.75	3.369; 3.385	97

				I4/mmm				
State	a (Å)	b (Å)	c (Å)	Fe-Fe (Å)	Fe-As (Å)	As-As (Å)	Ba-As (Å)	E_d (meV/Fe)
NM	3.944	3.944	12.470	2.79	2.32	3.70; 3.79	3.37	0
Expt.	3.960	3.960	13.010	2.80	2.40	3.74; 4.03	3.38	78

ever, there is not much known about the electronic structure and phonon modes corresponding to the low-temperature *Fmmm* phase in the AFM ground state. Here we carried out band calculations on $BaFe_2As_2$ having *Fmmm* symmetry. The energy bands corresponding to the NM and AFM2 states are calculated in the primitive cell of the optimized structure shown in Fig. 1. In order to reveal the effects of different atomic layers on the electronic structure, we also calculate the bands of individual Ba and Fe_2As_2 layers having the same atomic configuration in the optimized primitive cell. In addition to these the band structures of the AFM2 and AFM3 ground states calculated in the conventional cell are indicated in Fig. 1. The orbital-projected state densities and resulting total density of states (TDOS) of the AFM (AFM3) ground state is given to identify the character of bands. Energy bands together with the density of states in Fig. 2 provide a detailed information for the electronic structure of the *Fmmm* phase.

The energy bands of $BaFe_2As_2$ crystal near the Fermi level ($E_F=0$) is dominated by the bands of Fe_2As_2 layers. In fact, one can trace the bands of individual Fe_2As_2 layer in the band structure of $BaFe_2As_2$. However, this is not the case for the bands of the individual Ba layer despite their seemingly isolated configuration in $BaFe_2As_2$ crystal. The states due to Ba atoms are shifted to lower energies due to significant charge transfer from Ba to As atoms as demonstrated by the charge distribution analysis later in this section. The contribution of Ba orbitals to the filled states between E_F and −5 eV is rather small, but becomes significant between −15 and −10 eV. In fact, Ba-$4p$ orbitals give rise to a pronounced peak at approximately −15 eV in TDOS. Both structures, namely the NM and the AFM2 states of $BaFe_2As_2$ are metallic, but their energy bands are significantly different. Note that the crystal structure, magnetic order, and electronic structure of $BaFe_2As_2$ (Ref. 22) and $SrFe_2As_2$ (Ref. 23) are affected by pressure. For the NM state, the flat band between Γ-Z direction of the BZ becomes above Fermi level,

if the band structure were calculated using experimental lattice parameters. However, this band occurs below the Fermi level as in Fig. 2(c), since the optimized lattice parameters are used.

The bands of AFM2 presented in the conventional cell as presented in Fig. 2(e) are different from those of the AFM ground state (namely, AFM3) presented in Fig. 2(f). The flat band just below the Fermi level of the AFM3 state in Fig. 2(f) gives rise to a sharp peak in the total density of states close to the Fermi level. However, this peak is sharper in the AFM2 state. The states of this band originate from the strongly localized Fe-$3d_{xy}$ orbitals. Hybridization of Fe-$3d$ orbitals with As-$4p$ orbitals is minute in the states of this particular flat band, but becomes crucial for the states between −4 and −1 eV. While the contribution of Fe-$3d$ orbitals in the states between −6 and −4 eV recedes, the contribution of As-$4p$ orbitals increases.

The Fermi surface of $BaFe_2As_2$ in the nonmagnetic $I4/mmm$ symmetry consists of two holelike orbitals near the zone center and two electronlike orbitals near X point. This is in agreement with the results of angle-resolved photoemission spectroscopy (ARPES).[24] The Fermi surface of the AFM ground state constructed from the calculated electronic structure consists of four separated sheets at the four edges of the Brillouin zone, which are combined to nonuniform tubes leading to holelike orbitals and a single circular tube along Z-Γ-Z direction leading to electronlike orbitals.

C. Phonons

The magnetic properties and superconductivity of Fe-pnictide compounds exhibit strong sensitivity to the lattice and hence to the corresponding phonon spectrum.[25,26] Here we carried out magnetic phonon calculations of $BaFe_2As_2$ crystal for the AFM (AFM3) ground state at the Γ point of the conventional cell. In these calculations we used the optimized lattice parameters and determined the infrared (IR)
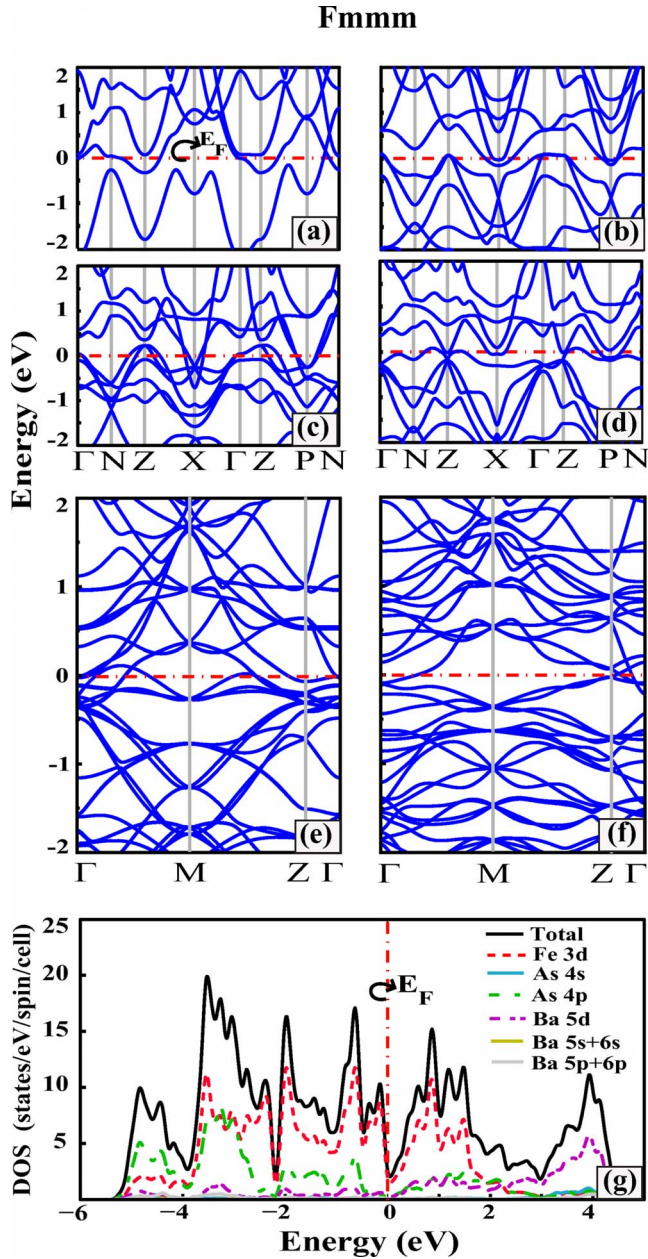
Fmmm

FIG. 2. (Color online) Energy-band structures of individual Ba (a) and Fe_2As_2 layers (b) together with the energy bands of the $BaFe_2As_2$ crystal in *Fmmm* symmetry corresponding to NM state (c) and AFM2 (d) states are calculated for the primitive cell of the optimized structure. Bands of the AFM2 state (e) and AFM ground state (AFM3) (f) both calculated in the conventional cell. (g) TDOS of the optimized AFM3 state together with orbital-projected DOS. The energy-band calculation of the NM state is carried out using optimized lattice parameters given in Table I.

and Raman-active (R) modes. Calculations are performed using the density-functional perturbation theory with plane-wave methods as implemented in PWSCF package.[13] Our results are presented in Table II. While Ba atoms contribute to the low-energy part of the calculated spectrum at Γ point, Fe and As atoms contribute to the frequency range 10–37 meV of the spectrum. The *Fmmm* phase has six Raman-active modes. In this respect, the IR data are crucial, since they can

provide reliable information about the atomic structure. The analysis of symmetry and frequency shows that E_u and E_g modes of $I4/mmm$ phase are doubly degenerate for normal phase, but are split under the applied pressure or collapse of c axis. These modes are also nondegenerate in the *Fmmm* phase.

Using inelastic neutron scattering, Mittal *et al.*[27] measured the temperature dependence of the phonon density of states of $BaFe_2As_2$ and determined the Raman-active modes. They also performed calculations of phonon spectrum for the non-magnetic state. Our results are in fair agreement with the experimental data on Raman-active modes.[25,27] We are predicting a phonon peak at 20 meV using spin-polarized calculation, which originates from vibrations of As atoms in *Fmmm* phase. This mode is observed experimentally at 21.5 meV,[27] but is not predicted by direct method with nonmagnetic calculations.[26] Earlier, phonon-dispersion curves of LaOFeAs have been obtained by Boeri *et al.*[28] and Singh *et al.*[29] In addition, Zbiri *et al.*[26] have obtained Raman-active modes for *Fmmm* and $I4/mmm$ phases of $BaFe_2As_2$ by non-magnetic calculations using experimental lattice parameters. Present results indicate however that the phonon spectrum of $BaFe_2As_2$ cannot properly be described by nonmagnetic phonon calculations which are performed using experimental lattice parameters.

As for IR-active modes, until now there is no theoretical treatment for the antiferromagnetic spin configuration of $BaFe_2As_2$ crystal. Experimentally, at the zone center, an IR-active Fe-As out-of-plane vibration mode is observed at $\sim$35 meV.[25] We are predicting this mode at 33.28 meV. Note that our results indicate softening and shift of some modes. As seen in Table II, almost all of Raman and IR frequencies are softened to smaller values when the effect of magnetic order is taken into account in phonon calculations.[30] For example, IR-active E_u modes of Fe in $I4/mmm$ are lowered from 36.45 and 36.79 meV to 34.82 and 32.71 meV in *Fmmm*. The Fe and As B_{2g} Raman modes show a giant phonon softening: Raman-active E_g modes of As in $I4/mmm$ are lowered from 18.31 and 19.20 meV to 13.93 and 18.52 meV B_{2g} and B_{3g} modes in *Fmmm*, respectively. Similarly, Raman-active E_g modes of Fe in $I4/mmm$ are lowered from 32.624 and 37.64 meV to 31.43 and 32.55 meV B_{2g} and B_{3g} modes in *Fmmm*, respectively. All these results show spin-lattice interaction in the structural phase transition from the high temperature to the low-temperature phase as found earlier by Yildirim[6] for LaOFeAs and by Hou *et al.*[31] for $BaFe_2As_2$.

D. Analysis of charge distribution

The analysis of charge distribution is carried out to reveal valuable information about the character of the bonding and basic features of the structures. In spite of ambiguities in determining the rigorous values, the calculation of charge transfer between atoms or atomic layers may be useful in understanding the system under consideration. Here we present the isosurfaces of total charge density of the AFM ground state in the conventional cell in Fig. 3. In the same figure the counterplots of the total charge are also shown on

TABLE II. Calculated frequencies of Raman-active (R) and IR-active modes (in meV) of *Fmmm* and *I4/mmm* phases at the Γ point and their symmetry analysis. The subscripts u and g represent antisymmetric and symmetric vibrations, respectively. The other subscript i (i = 1, 2, 3) indicates the stretching modes. Modes of the AFM ground state corresponding to AFM3 spin configuration are calculated in the conventional cell with optimized lattice parameters. As for the phonon modes, specified as AFM3 (expt.) and NM (expt.), are calculated by using experimental lattice constant with experimental As coordinate, z_{As}.

	Fmmm	
Atom	Wyckoff position	Phonon modes
Ba	$4a$	$B_{1u}+B_{2u}+B_{3u}$
Fe	$8f$	$B_{1g}+B_{2g}+B_{3g}+B_{1u}+B_{2u}+B_{3u}$
As	$8i$	$A_g+B_{1u}+B_{2u}+B_{3u}+B_{2g}+B_{3g}$

$$\text{Raman}=A_g+B_{1g}+2B_{2g}+2B_{3g}$$
$$\text{IR}=3B_{1u}+3B_{2u}+3B_{3u}$$

State	IR (meV)	R (meV)
AFM3 (Expt.)	$B_{1u}(10.94,32.59)$; $B_{2u}(29.32,37.59)$; $B_{3u}(27.88,32.71)$	$A_g(25.82)$, $B_{1g}(26.33)$; $B_{2g}(12.71,32.26)$; $B_{3g}(18.64,35.0)$
AFM3	$B_{1u}(11.36,33.28)$; $B_{2u}(30.26,34.82)$; $B_{3u}(27.85,32.71)$	$A_g(26.061)$, $B_{1g}(27.57)$; $B_{2g}(13.93,31.434)$; $B_{3g}(18.52,32.55)$

	I4/mmm	
Atom	Wyckoff position	Phonon modes
Ba	$2a$	$A_{2u}+E_u$
Fe	$4d$	$B_{1g}+E_g+A_{2u}+E_u$
As	$4e$	$A_{1g}+A_{2u}+E_g+E_u$

$$\text{Raman}=2E_g+A_{1g}+B_{1g}$$
$$\text{IR}=3A_{2u}+3E_u$$

State	IR (meV)	R (meV)
NM	$A_{2u}(11.52,33.99)$, $E_u(17.87,18.17,36.45,36.79)$	$E_g(18.31,19.20,36.24,37.64)$, $A_{1g}(26.55)$, $B_{1g}(27.48)$
NM (expt.)	$A_{2u}(10.92,33.64)$, $E_u(15.80,30.08)$	$E_g(16.79,30.47)$, $A_{1g}(25.79)$, $B_{1g}(27.22)$

the specific planes. Isosurfaces of the total charge clearly show the bonds between As atoms in the (100) plane. The counterplots of charge density on the (100) plane quantify these isosurface plots on the faces of orthorhombic cell. However, neither isosurface, nor contour plots calculated on the (100) plane present any evidence for directional (covalent) bonding between Ba and As atoms. Such a bond is also absent between two As atoms below and above the Ba atomic layer. The low value of charge density (0.005 unit) between As atoms above and below Ba atom is actually due to the metallic charge in the Ba layer. In the case of collapse (nonmagnetic) phase of $BaFe_2As_2$ crystal the bond between these As ions do not occur due to the interaction between Ba ions and As ions.

The metallic bond between Ba atoms within the Ba layers is revealed only if the isosurface values were lowered. It is, however, clearly seen in the charge density counterplots on the (110) plane. High charge density around Fe ions is due to Fe-$3d$ orbitals. Each Fe atom forms four Fe-As bonds in tetrahedral directions, which are achieved through the hybridization of Fe-$3d$ and As-$4p$ orbitals. Even if one cannot

calculate rigorously, the charge transfer from Fe to As atoms (which is estimated to be 0.16 electrons using Bader scheme)[32] attributes a minute ionic character to the four Fe-As bonds. Our charge density analysis based on Bader scheme also estimates that 1.24 electrons are transferred from Ba atoms. Considering the charge transferred from Fe and Ba atoms, the excess charge on the As atoms amounts to 0.78 electrons. Moreover, Mulliken[33] population analysis indicates that the Mulliken charge of Ba, Fe, and As in $BaFe_2As_2$ crystal in the AFM ground state were approximately, +1.20, +0.26, and −0.86, respectively. These values corroborate the charge-transfer values revealed by Bader analysis and both Bader and Mulliken charge analyses demonstrate that electrons are transferred from Ba layer to FeAs layer.

Despite the ambiguities in quantitative determination of the charge transfer between constituent atoms, critical information can be revealed from the calculation of the difference charge density. We first plot the difference charge density obtained by subtracting the charges of Fe-As and Ba layers from the total charge density of the AFM ground state,
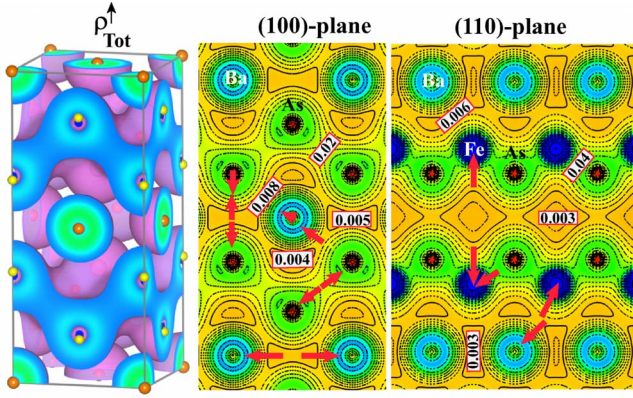
FIG. 3. (Color online) Charge distribution of the *Fmmm* phase in the AFM ground state. Left: Total charge-density isosurface plots in the conventional cell with isosurface value of 0.0012 electrons/Å^3. Middle: contour plots calculated on the (100) plane (i.e., one of the side faces of the conventional cell). Right: Contour plots on the (110) plane. In the counterplots, the charge density increases along the direction indicated by small arrows. Numerals in the counterplots indicate the values of charge density in units of at the specific locations.
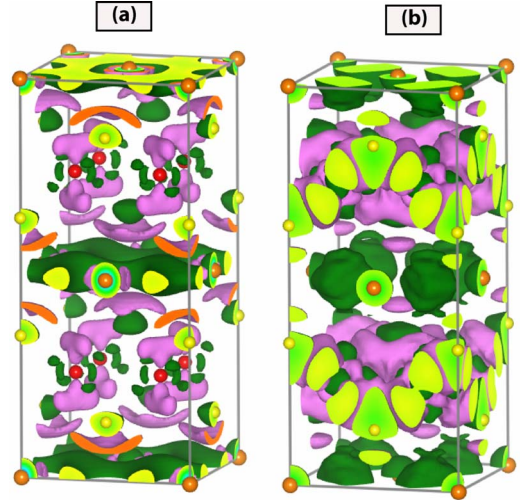

FIG. 4. (Color online) Top panels: (a) Isosurface plots of the difference charge density $\Delta\rho_L$ calculated by subtracting the charge densities of individual FeAs and Ba layers from the total charge density of the AFM ground state. (b) Isosurface plots of the difference charge density $\Delta\rho_A$ calculated by subtracting the charge densities of the constituent free atoms from the total charge density. Pink-light and green-dark isosurface plots are for positive and negative values, respectively. Isosurface value is 0.0012 electrons/Å^3

namely $\Delta\rho_L = \rho_T - \rho_{\text{FeAs}} - \rho_{\text{Ba}}$. As mentioned in Sec. III B, we considered Ba and FeAs layers as if the ingredients of the BaFe$_2$As$_2$ iron-pnictide crystal, and calculated the charge density of each layer individually in the same unit cell keeping their atomic structure the same as in BaFe$_2$As$_2$ crystal. In these plots negative values of the difference charge density indicate the depletion of the electrons from the layer. The positive values are interpreted as the accumulation of excess electrons to the layer. Isosurface plots of calculated difference charge density, $\Delta\rho_L$, are presented in Fig. 4(a). Dark (green) isosurfaces show the charge transfer from the Ba layers to the pink (light) isosurfaces of FeAs layers. In Fig. 4(b) we calculate the isosurface plots of the difference charge density, which are obtained by subtracting the charge densities of the constituent free atoms (Ba, Fe, and As) located in the positions equivalent to their positions in the crystal, namely, $\Delta\rho_A = \rho_T - \rho_{\text{Ba}} - \rho_{\text{Fe}} - \rho_{\text{As}}$. Charge depletion on Ba and Fe atoms and charge accumulation on As atoms are clearly seen.

IV. CONCLUSIONS

In conclusion, we presented a theoretical study of the undoped iron-pnictide BaFe$_2$As$_2$ crystal based on first-principles plane-wave calculations within density-functional theory. Our analysis comprises atomic, electronic, and magnetic structures, as well as phonon modes at the center of the Brillouin zone. While our study is focused on the orthorhombic *Fmmm* phase, we also considered the tetragonal *I*4/*mmm* phase for the sake of completeness. Among different spin configurations we determined the magnetic ground state of the *Fmmm* phase. The complex spin configuration of this ground state agrees with the experimental results, but differs from that of the antiferromagnetic state achieved by the antiparallel spin alignment on two Fe atoms in the primitive unit cell. We found that the electronic state density of the antiferromagnetic ground state close to the Fermi level is characterized by a sharp peak, which is derived mainly from Fe-3d_{xy} orbitals with a small contribution from the As-4p orbitals. Whereas states originating from Ba orbitals become pronounced at the lower part of the spectrum. The analysis of charge transfer reveals valuable information about charge states and bonding between atoms. The magnetic phonon calculations are essential to distinguish the correct spin configuration. Our analysis of the phonon modes of the AFM ground state at the Γ point predicts Raman- and IR-active modes, some of which were softened.

ACKNOWLEDGMENTS

*ciraci@fen.bilkent.edu.tr

[1] Y. Kamihara, T. Watanabe, M. Hirano, and H. Hosono, J. Am. Chem. Soc. **130**, 3296 (2008).

[2] M. Rotter, M. Tegel, and D. Johrendt, Phys. Rev. Lett. **101**, 107006 (2008).

[3] P. L. Alireza, Y. T. Chris Ko, J. Gillett, C. M. Petrone, J. M. Cole, G. G. Lonzarich, and S. E. Sebastian, J. Phys.: Condens. Matter **21**, 012208 (2009).

[4] M. Rotter, M. Tegel, D. Johrendt, I. Schellenberg, W. Hermes, and R. Pöttgen, Phys. Rev. B **78**, 020503(R) (2008).

[5] J. K. Dong, L. Ding, H. Wang, T. Wu, X. H. Chen, and S. Y. Li, New J. Phys. **10**, 123031 (2008).

[6] T. Yildirim, Phys. Rev. Lett. **101**, 057010 (2008).

[7] Q. Huang, Y. Qiu, W. Bao, M. A. Green, J. W. Lynn, Y. C. Gasparovic, T. Wu, G. Wu, and X. H. Chen, Phys. Rev. Lett. **101**, 257003 (2008).

[8] Y. Su, P. Link, A. Schneidewind, Th. Wolf, P. Adelmann, Y. Xiao, M. Meven, R. Mittal, M. Rotter, D. Johrendt, Th. Brueckel, and M. Loewenhaupt, Phys. Rev. B **79**, 064504 (2009).

[9] R. A. Ewings, T. G. Perring, R. I. Bewley, T. Guidi, M. J. Pitcher, D. R. Parker, S. J. Clarke, and A. T. Boothroyd, Phys. Rev. B **78**, 220501(R) (2008).

[10] W. Z. Hu, J. Dong, G. Li, Z. Li, P. Zheng, G. F. Chen, J. L. Luo, and N. L. Wang, Phys. Rev. Lett. **101**, 257005 (2008).

[11] T. Yildirim, Phys. Rev. Lett. **102**, 037003 (2009).

[12] J. P. Perdew, K. Burke, and M. Ernzerhof, Phys. Rev. Lett. **77**, 3865 (1996).

[13] S. Baroni, A. Del Corso, S. Girancoli, and P. Giannozzi, http://www.pwscf.org/

[14] H. J. Monkhorst and J. D. Pack, Phys. Rev. B **13**, 5188 (1976).

[15] E. R. Davidson, J. Comput. Phys. **17**, 87 (1975).

[16] I. A. Nekrasov, Z. V. Pchelkina, and M. V. Sadovskii, JETP Lett. **88**, 144 (2008).

[17] D. J. Singh, Phys. Rev. B **78**, 094511 (2008).

[18] F. Ma, Z.-Y. Lu, and T. Xiang, Phys. Rev. B **78**, 224517 (2008).

[19] I. R. Shein and A. L. Ivanovskii, Phys. Rev. B **79**, 054510 (2009).

[20] C. Krellner, N. Caroca-Canales, A. Jesche, H. Rosner, A. Ormeci, and C. Geibel, Phys. Rev. B **78**, 100504(R) (2008).

[21] G. Xu, H. Zhang, X. Dai, and Z. Fang, EPL **84**, 67015 (2008).

[22] W. Xie, M. Bao, Z. Zhao, and B.-G. Lui, Phys. Rev. B **79**, 115128 (2009).

[23] M. Kumar, M. Nicklas, A. Jesche, N. Caroca-Canales, M. Schmitt, M. Hanfland, D. Kasinathan, U. Schwarz, H. Rosner, and C. Geibel, Phys. Rev. B **78**, 184516 (2008).

[24] L. X. Yang, H. W. Ou, J. F. Zhao, Y. Zhang, D. W. Shen, B. Zhou, J. Wei, F. Chen, M. Xu, C. He, X. F. Wang, T. Wu, G. Wu, Y. Chen, X. H. Chen, Z. D. Wang, and D. L. Feng, Phys. Rev. Lett. **102**, 107002 (2009).

[25] D. Reznik, K. Lokshin, D. C. Mitchell, D. Parshall, W. Dmowski, D. Lamago, R. Heid, K.-P. Bohnen, A. S. Sefat, M. A. McGuire, B. C. Sales, D. G. Mandrus, A. Asubedi, D. J. Singh, A. Alatas, M. H. Upon, A. H. Said, Yu. Shvyd'ko, and T. Egami, arXiv:0810.4941 (unpublished).

[26] M. Zbiri, H. Schober, M. R. Johnson, S. Rols, R. Mittal, Y. Su, M. Rotter, and D. Johrendt, Phys. Rev. B **79**, 064511 (2009).

[27] R. Mittal, Y. Su, S. Rols, T. Chatterji, S. L. Chaplot, H. Schober, M. Rotter, D. Johrendt, and Th. Brueckel, Phys. Rev. B **78**, 104514 (2008).

[28] L. Boeri, O. V. Dolgov, and A. A. Golubov, Phys. Rev. Lett. **101**, 026403 (2008).

[29] D. J. Singh and M.-H. Du, Phys. Rev. Lett. **100**, 237003 (2008).

[30] Note that specific modes such as E_u IR-active modes of As in the xy plane of $I4/mmm$ phase is increased to 30.26 meV in *Fmmm* phase.

[31] D. Hou, Q. M. Zhang, Z. Y. Lu, and J. H. Wei, arXiv:0901.1525 (unpublished); in this work, the phonon calculation was performed using experimental lattice constant.

[32] G. Henkelman, A. Arnaldsson, and H. Jonsson, Comput. Mater. Sci. **36**, 354 (2006).

[33] R. S. Mulliken, J. Chem. Phys. **23**, 1833 (1955).